

Evaluation of digital methods for energy calculation and timing pick-off in positron emission tomography

To cite this article: H.M. Murata *et al* 2018 *JINST* **13** P09024

View the [article online](#) for updates and enhancements.



IOP | ebooks™

Bringing you innovative digital publishing with leading voices to create your essential collection of books in STEM research.

Start exploring the collection - download the first chapter of every title for free.

Evaluation of digital methods for energy calculation and timing pick-off in positron emission tomography

H.M. Murata,^{a,1} M. Morales^b and D.A.B. Bonifácio^a

^a*Instituto de Radioproteção e Dosimetria, IRD-CNEN/RJ
Avenida Salvador Allende, s/n, 22783-127, Rio de Janeiro, RJ, Brazil*

^b*Instituto de Pesquisas Energéticas e Nucleares, IPEN-CNEN/SP
Avenida Lineu Prestes, 2242, 05422-970, São Paulo, SP, Brazil*

E-mail: heliomurata@gmail.com

ABSTRACT: Traditionally, pulse processing in Positron Emission Tomography (PET) has been based on analog or discrete circuits forming a decentralized processing system. However, there is a convergence for digital and integrated implementations due to the characteristics of the modern electronic devices which are real-time processing capable, such as Application-Specific Integrated Circuit (ASIC) and Field Programmable Gate Array (FPGA) with fast Analog to Digital Converters (ADC). However, FPGA can provide fast implementation at relatively low cost and also enables the development of sophisticated digital pulse processing algorithms to improve energy, position and time resolutions in PET systems. Our group has developed and evaluated one energy calculation and three timing pick-off methods for implementation onto an FPGA-based system. For a typical PET detector setup, our charge integration method presents energy resolution similar to previously designed PET detectors. The best performance for timing pick-off was achieved by the Initial Rise Interpolation (IRI) method, where a coincidence time resolution of around 440 ps is suitable for Time of Flight (TOF) PET. Future works include embedding the proposed algorithms in a FPGA-based data acquisition system under development by our group which will be employed in a PET prototype.

KEYWORDS: Data acquisition circuits; Data processing methods; Digital electronic circuits; Gamma camera, SPECT, PET PET/CT, coronary CT angiography (CTA)

¹Corresponding author.

Contents

1	Introduction	1
2	Materials and methods	2
2.1	Experimental setup	2
2.2	Algorithm design and evaluation	3
2.2.1	Baseline	3
2.2.2	Energy calculation	3
2.2.3	Timing analysis	4
3	Results and discussion	5
3.1	Acquisition of energy spectra	5
3.2	Coincidence timing measurement	7
4	Conclusions	9

1 Introduction

Positron Emission Tomography (PET) [1] is a nuclear imaging modality used for *in vivo* evaluation of metabolic activity. This technique is based on the administration of a certain amount of a molecule into a living organism. This molecule, named radiopharmaceutical, is labeled with a positron-emitting radionuclide. After losing its kinetic energy, the positron annihilates with an electron, producing two 511 keV photons emitted in opposite directions. The PET detection system involves multiparametric acquisition and requires the determination of arrival time, position of interaction and deposited energy for each event. The detected photons are processed by a coincidence system, resulting in spatial and temporal distributions of the radiopharmaceutical metabolized by the live organism.

In addition to the usual scintillator-based detectors [2, 3], new approaches in PET detectors have been developed to improve the timing performance, such as those using the compound semiconductor TlBr coupled to SiPMs [4]. More recently, the digital Silicon Photomultiplier (dSiPM) has been proposed to improve timing resolution in PET [5, 6]. However, the high Dark Current Rates (DCR) of dSiPM devices still remain an issue to be solved [7, 8].

Traditionally, pulse processing in PET has been based on analog or discrete circuits forming a decentralized processing system. However, there is a convergence for digital implementations due to several favorable characteristics of the currently available electronic components. Combining high sampling rate and high bit resolution Analog to Digital Converters (ADC) and Field Programmable Gate Array (FPGA) devices provide solutions with simultaneous computing and real-time processing capabilities [9]. Modern PET systems are also using Application-Specific Integrated Circuit (ASIC) for photodetector readout [10, 11]. However, unlike ASIC, FPGAs are reconfigurable allowing for a fast implementation at relatively low cost [12–14]. The centralization

of the digital processing onto a single FPGA device simplifies the electronics, since several features can be embedded in a system consisting of processors, memories and, input/output peripherals [14].

The use of FPGA technology also enables the development of sophisticated digital pulse processing algorithms to improve energy, position and time resolutions in PET systems [15–20], which results in better image quality. For instance, improvements in energy and coincidence time resolutions, as required by Time of Flight (TOF) PET system [21, 22] provides better precision at the positioning of the annihilation event along the Line of Response (LOR), enhancing the Signal-to-Noise Ratio (SNR) of the reconstructed image.

In PET, energy information is used to separate the photons that have not undergone scattering and is usually obtained by measuring the charge or pulse amplitude from the photodetector. In a digital approach, a typical implementation to calculate the energy is performed by integrating the pulse in a determined time interval with baseline subtraction.

Analog standard timing methods can be digitally processed, including digital Leading-Edge Discrimination (dLED) [23]. However, other methods, such as the Maximum Rise Interpolation (MRI) [24] and the Initial Rise Interpolation (IRI) [19] are developed exclusively for digital pulse processing and aim to achieve an optimized coincidence time resolution.

Our group has developed one energy calculation and three timing pick-off methods for implementation onto an FPGA-based system. In this work, the algorithms are described and their performances are evaluated with experimental data acquired by a high sampling rate digitizer.

2 Materials and methods

2.1 Experimental setup

Experimental data was acquired from a setup consisting of a ^{22}Na calibration source (395 kBq) placed between two LYSO (Proteus, U.S.A.) crystals ($3 \times 3 \times 20 \text{ mm}^3$) for coincidence detection at 180° , as shown in figure 1.

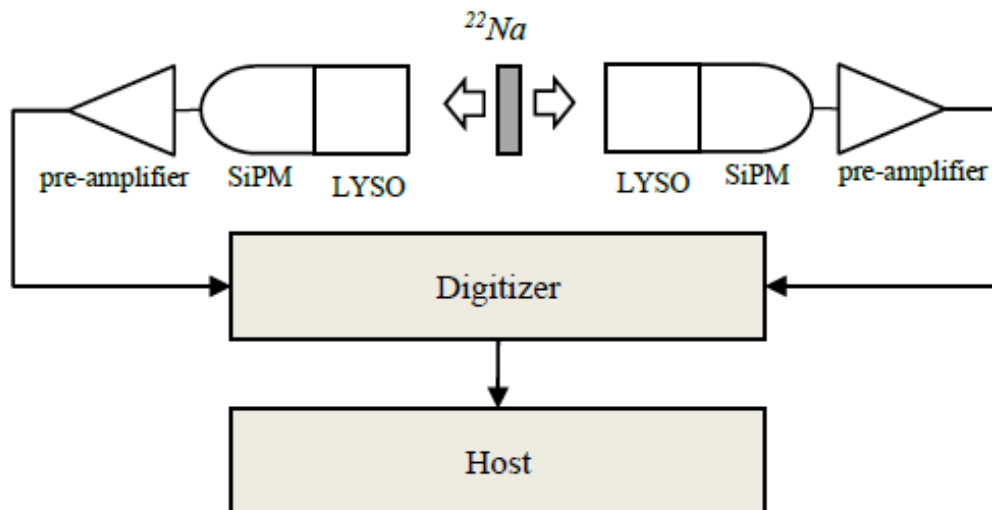


Figure 1. Schematic diagram of the setup for data acquisition and pulse processing.

The distance between the crystals was 15 mm and each one was coupled to a 3×3 mm² SiPM (or MPPC — Multi Pixel Photon Counter) model S1031-025P (Hamamatsu, Japan). The electric signals from the SiPM's were pre-amplified before being digitized by the v1720 digitizer (CAEN, Italy) with a 12-bit resolution ADC at 250 MS/s.

The digitizer was loaded with a firmware that provides energy calculation by charge integration and timing pick-off by using a proprietary digital pulse processing algorithm. Besides the charge and time information, this firmware also allows the acquisition of the pulse waveform by activating the “mixed-mode” [25]. Using the libraries provided by the digitizer manufacturer, a custom software was developed for the acquisition of the complete pulse.

2.2 Algorithm design and evaluation

Quartus Prime Standard Edition version 16.1 (Intel, U.S.A.) was used for the algorithm design, which was described in Very High Speed Integrated Circuits Hardware Description Language (VHDL). The design was verified by functional simulation in ModelSim Starter Edition version 10.5b (Intel, U.S.A.). The FPGA target was an Intel Arria 10 device with 270,000 Logic Elements (LE). The algorithm in Matlab (MathWorks, U.S.A.) was also developed using low complexity logic to validate the results provided by the VHDL design.

2.2.1 Baseline

The baseline is the current level to which the pulse decays [26]. The baseline was calculated as the average of the first n samples before the pulse leading edge (eq. (2.1)):

$$\text{baseline} = \frac{1}{n} \sum_{i=0}^{n-1} s_i \quad (2.1)$$

In this work, the number of samples to calculate the baseline n was set to 64 samples.

2.2.2 Energy calculation

The photodetector response to the scintillation photons is a current that flows during a period equal to the charge collection time. The total amount of generated charge (Q) is the time integral over the duration of the current [27]. The charge released in the photodetector is proportional to the energy of gamma rays photons absorbed in the scintillator. In the digital approach, the charge for each event consists of summing the digitized voltage sample values (s_j) within a single integration window and subtracting the resulting value from the baseline (eq. (2.2)):

$$Q = \sum_{j=g_i}^{g_f} (s_j - \text{baseline}) \quad (2.2)$$

where g_i and g_f denotes the first and last samples of the integration window, respectively. In this work, the size of the integration window was set to 35 samples (i.e., $g_f - g_i + 1 = 35$). This integration window corresponds to a time interval of 140 ns due to the ADC sampling rate at 250 MS/s, which is equivalent to 4 ns per sample. Charge values for each event were calculated by algorithms in VHDL and Matlab from the waveform acquired by the digitizer (eq. (2.2)).

The performance of the proposed energy calculation algorithm was compared against the built-in digitizer solution. The energy spectrum of the collected photons (histogram of pulse charges) generated by the digitizer was compared against spectra calculated by both algorithms developed in this work. All spectra were linearly calibrated by the 511 keV photopeak, which was assumed as a Gaussian distribution. An energy selection within a window from 356 to 670 keV was used to fit a linear background below the photopeak. This linear fit was subtracted from the photopeak region to fit a Gaussian function. The Full Width at Half Maximum (FWHM) was calculated based on the Gaussian fit.

2.2.3 Timing analysis

The arrival time of each pulse was calculated by crossing the threshold (dLED) or by the crossing time of the baseline point (MRI and IRI) with the interpolated line formed by two subsequent samples. For all methods, the trigger is generated when a sample exceeds a threshold level.

The digitizer provides a built-in threshold-crossing method for timing based on Leading-Edge Discrimination (LED). In this method, the arrival time t_{ref} is stamped at the trigger sample t_{trg} ($t_{ref} = t_{trg}$). The trigger sample is the first sample over the threshold level in the pulse leading edge; i.e., t_{ref} is always a multiple of 4 ns. Figure 2 exhibits the functional block diagram of the timing and charge calculation for each pulse.

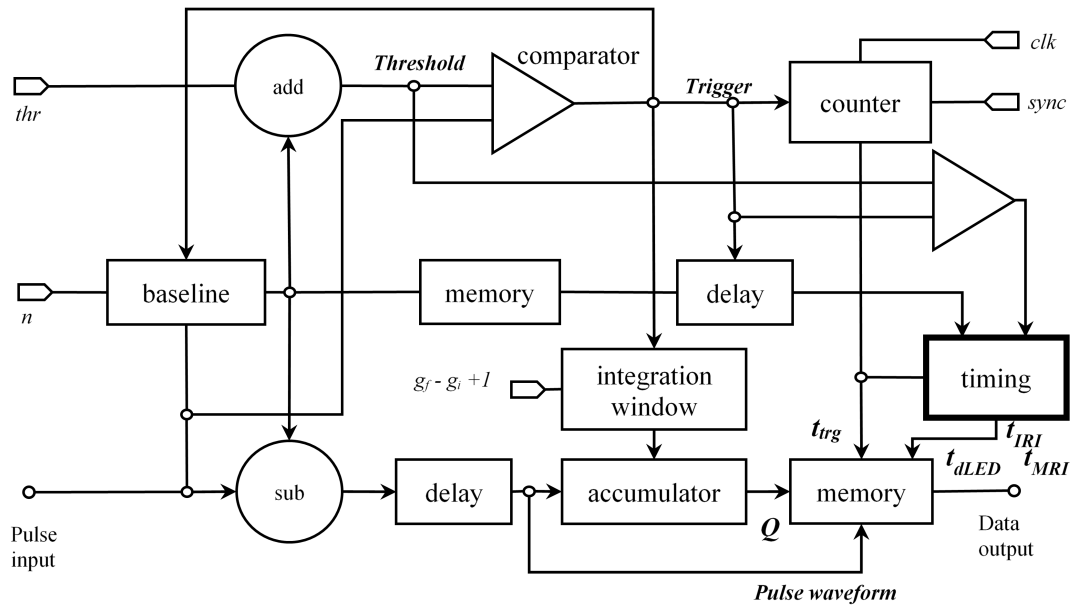


Figure 2. Block diagram for charge calculation (Q), trigger time stamp (t_{trg}) and timing process (t_{dLED} , t_{IRI} and t_{MRI}) for each event.

The built-in timing pick-off algorithm of the digitizer firmware presents reduced performance for PET applications because the time values are estimated in multiples of 4 ns (from -8 ns to $+8$ ns). Therefore, the built-in firmware provides a poor resolution time difference distribution, which is not comparable to our developed algorithms. Hence, the three following described algorithms were compared for evaluation purposes regarding Coincidence Time Resolution (CTR) and time difference distribution.

Digital leading-edge discrimination. The LED is a widely method used in analog circuit approaches due to its simplicity. A trigger signal from a comparator output occurs when, using a comparator, the input signal crosses a discriminator threshold level, registering the arrival time of the pulse [23, 28]. In this threshold-crossing technique, the threshold level value must be assigned considering the probability of triggering noise pulses and possible issues with timing jitter and time walk [16, 28].

Noise amplitude lies within a limit of 6σ peak to peak from a determined source, whereby the total noise is the root-mean-square (rms) value of all mean-square voltages of the individual noise sources. Low energy noise from other sources can trigger the digitizer [29]. With these considerations, the threshold level value was set to baseline $+210\text{ LSB}$, which corresponds to approximately the baseline $+6\sigma$, which is a value low enough to acquire most of the gamma pulses, but high enough to reduce the noise rate.

In the digital version of LED (dLED), the arrival time of the pulse is determined at the intersection of the threshold with the linear interpolation line between the trigger sample and previous sample (eq. (2.3)):

$$t_{\text{dLED}} = t_{\text{trg}} - 1 + (\text{threshold} - y(t_{\text{trg}} - 1)) / (y(t_{\text{ref}}) - y(t_{\text{trg}} - 1)) \quad (2.3)$$

Maximum rise interpolation. In the MRI method, the pulse timing is determined by calculating the baseline-crossing of the maximum rise line. The maximum rise line is the linear interpolation between two adjacent samples where the pulse rise has its maximum (eq. (2.4)):

$$t_{\text{MRI}} = t_{\text{trg}} - (y(t_{\text{trg}}) - \text{baseline}) / (y(t_{\text{trg}} + 1) - y(t_{\text{trg}})) \quad (2.4)$$

Initial rise interpolation. The IRI method is analogous to MRI, but the pulse timing is determined by calculating the baseline-crossing of the initial rise points of signal pulse (eq. (2.5)). The slope of the pulse at the leading edge is proportional to the influence of the sampling phase of the ADC clock and is smaller at initial rise than maximum rise [19]. In both techniques, the threshold discriminator was used to trigger the pulse at t_{trg} sample.

$$t_{\text{IRI}} = t_{\text{trg}} - 1 - (y(t_{\text{trg}} - 1) - \text{baseline}) / (y(t_{\text{trg}}) - y(t_{\text{trg}} - 1)) \quad (2.5)$$

Figure 3 shows the comparison of different timing methods for a digitized pulse.

3 Results and discussion

3.1 Acquisition of energy spectra

Figure 4 shows the ^{22}Na energy spectra acquired by the v1720 digitizer. The spectrum produced by the built-in digitizer firmware was used as a reference for the spectra from the VHDL and Matlab algorithms.

About 0.6% of the input signals computed as a pulse by the digitizer firmware were identified by our algorithm as noise or pile-up. These event data were excluded from the statistical analysis to avoid degradation in the energy spectrum.

Most of the discrepancies among the spectra are below 200 keV and they are due mainly to the differences between the baseline restoration algorithms from the reference and this work.

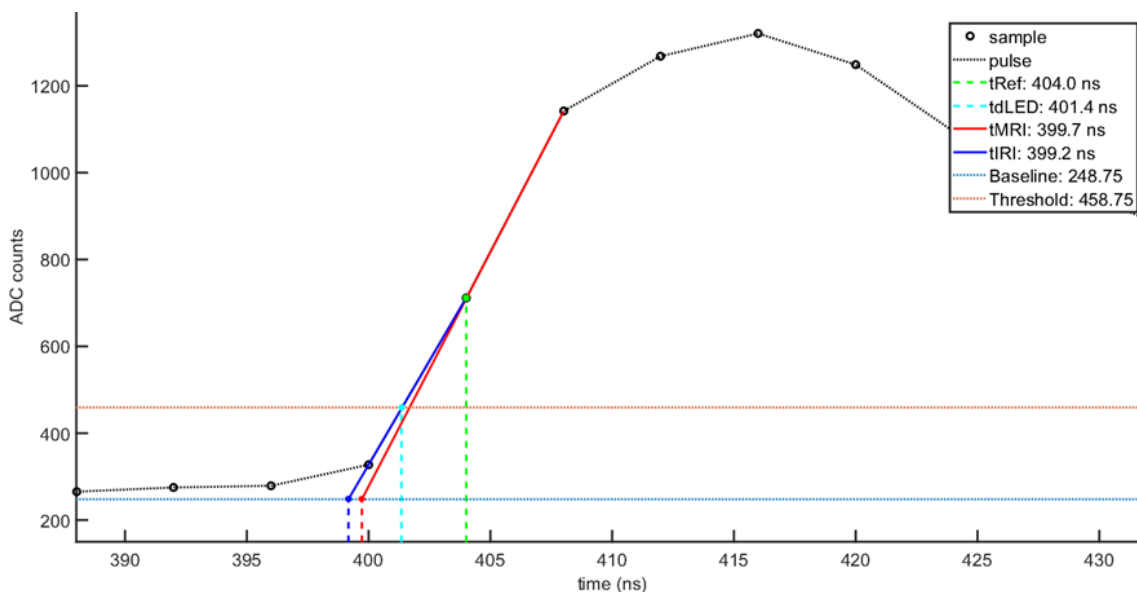


Figure 3. Pulse with application of dLED, MRI, IRI and the digitizer reference timing pick-off methods.

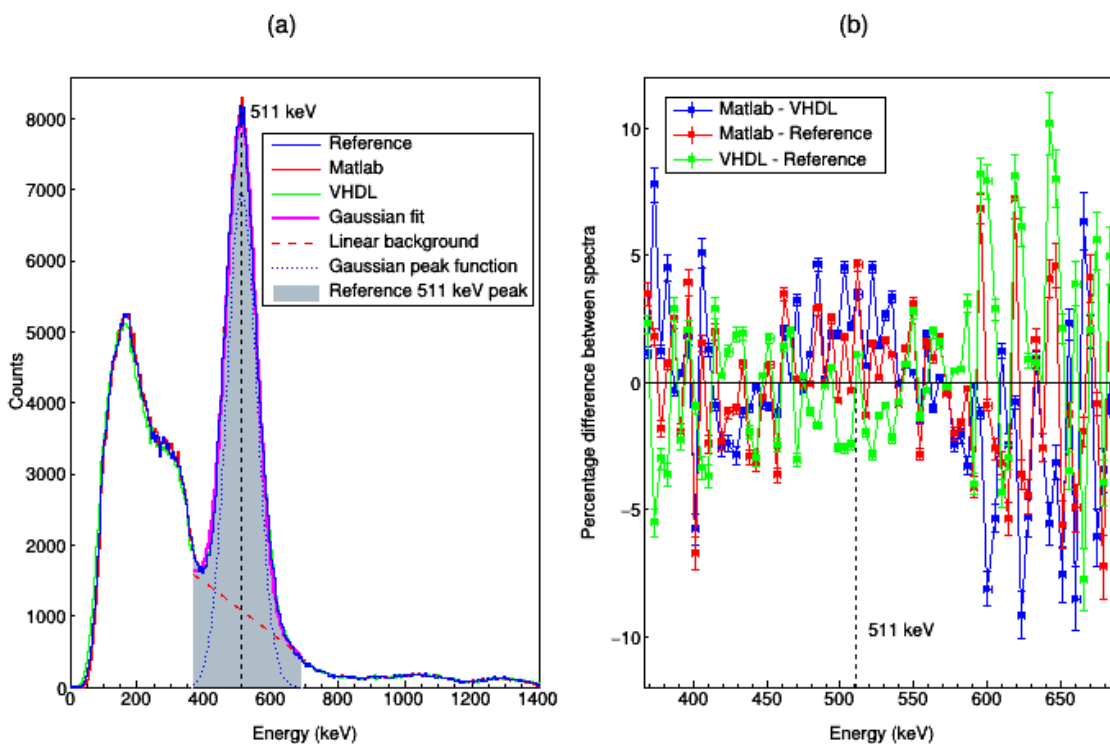


Figure 4. (a) ^{22}Na energy spectra of the LYSO scintillator coupled to a SiPM. Samples data were acquired by digitizer (reference) and processed in Matlab and VHDL. The Gaussian fit at the 511 keV peak considers a linear background. (b) Percentage differences between the three spectra at the 511 keV photopeak region.

Table 1. Values of the energy standard deviation (σ), FWHM and resolution based on a Gaussian fit at 511 keV peak with better as possible chi-squared over degrees of freedom (χ^2/η) test.

	σ (keV)	FWHM (keV)	Resolution (%)	χ^2/η
Reference	44, 50 \pm 0, 28	104, 80 \pm 0, 65	20, 51 \pm 0, 13	1,89
Matlab	43, 55 \pm 0, 27	102, 56 \pm 0, 64	20, 07 \pm 0, 13	1,98
VHDL	44, 65 \pm 0, 28	105, 14 \pm 0, 66	20, 58 \pm 0, 13	1,29

Table 1 shows the FWHM and energy resolution values based on a Gaussian fit at 511 keV peak with chi-squared over degrees of freedom (χ^2/η) test.

The 511 keV peak presents some Compton backscatter events and other noise sources. Obtained energy resolution values from the Matlab and VHDL algorithms indicate the accordance with the reference.

Energy resolution values obtained with this setup are similar to a typical PET detector module [30, 31]. As energy resolution is highly dependent on the type of detector being used, the recent PET application works show SiPM photodetectors coupled to LYSO crystal scintillators with energy resolution between about 14% and 22% FWHM at 511 keV [32–37].

3.2 Coincidence timing measurement

Coincidence mode acquisition was performed with a typical PET coincidence time window of 10 ns [38]. DLED, IRI and MRI and timing pick-off methods were applied for each registered event. Figure 5 exhibits the time difference distributions of the coincidence events. Distributions were generated both in Matlab and FPGA-based algorithms.

The lower sampling frequency rate significantly affects the use of the MRI method in fast leading edge rising [19, 39]. The use of the threshold to trigger an event causes divergent timestamp using the MRI method with low energy pulses, as shown in figure 6.

For PET applications, timing is not substantially influenced for pulses with amplitudes near the threshold level.

Table 2. FWHM timing resolution for different digital timing methods.

	Matlab	VHDL
Timing method	FWHM (ps)	FWHM (ps)
IRI	484 \pm 7	440 \pm 3
dLED	878 \pm 4	845 \pm 5
MRI	2098 \pm 15	2134 \pm 14

Studies using the MRI method with similar configuration showed similar FWHM values [24, 40]. In the Matlab simulation, the IRI method presented a timing resolution that was 45% better timing resolution than the dLED method and 77% better than the MRI method. In the VHDL design, the IRI method presented a resolution that was 48% better resolution than the dLED method and 79% better than the MRI, as already verified in previous studies [19].

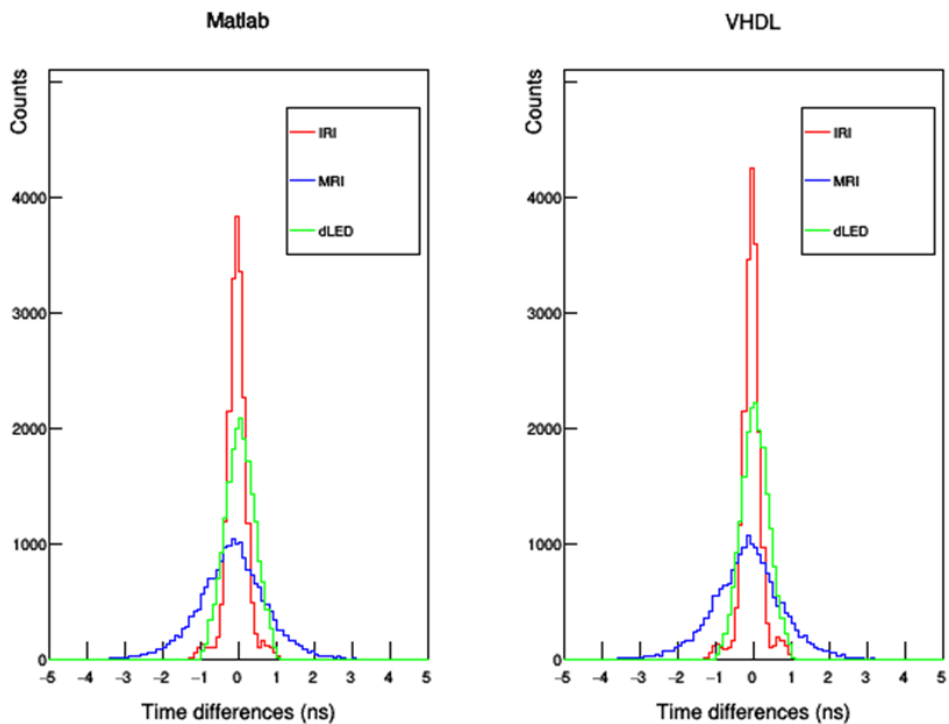


Figure 5. Distribution of time differences in coincidence using dLED, IRI and MRI timing methods simulated in Matlab and provided by FPGA-based algorithm in VHDL.

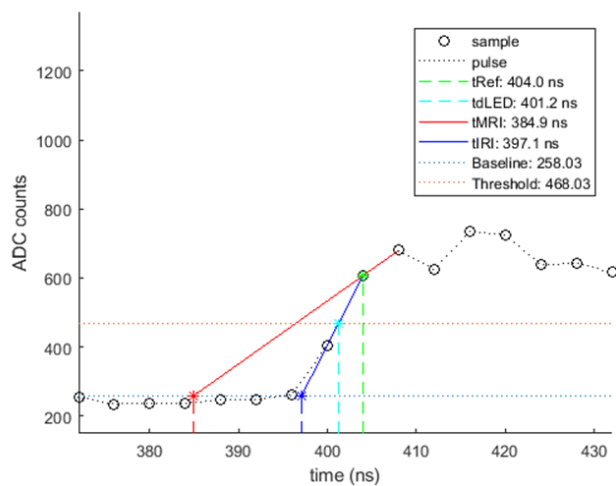


Figure 6. Divergent time stamp using MRI method due the use of threshold-crossing to trigger low energy pulses.

4 Conclusions

Our group has developed and evaluated FPGA algorithms for digital pulse processing in PET. All VHDL designs were successfully validated by the Matlab using low complexity algorithms. This study indicates the feasibility of low resources consumption and real-time capable FPGA algorithms to perform suitable energy and timing resolutions onto an FPGA platform for PET applications.

Our charge integration method presents energy resolution results in good agreement with a commercial digitizer used as reference, which are similar to previously designed PET detectors.

IRI and dLED methods presented subnanosecond CTR and are suitable for TOF PET. The best performance for timing pick-off was achieved by the IRI method, which presented around 440 ps CTR, and it should be considered an alternative choice in digital implementations.

Proposed energy calculation and timing pick-off algorithms will be embedded in an under development FPGA-based data acquisition module which will be employed in a PET detector block prototype. The detector block will be based on a monolithic scintillator crystal coupled to a SiPM array in a row-column summing readout scheme. All the signals from the readout will be digitized and processed onto a single FPGA device (figure 7) and their sum will be employed for energy calculation and timing pick-off [41]. In a complete PET system, an external clock is sent to the FPGAs through splitters to synchronize clock and start times for each FPGA [42]. Positioning algorithms with DOI capabilities will be considered [20, 43]. Our group has already developed a 3D positioning method [43] that produces similar results to existing works, but it does not require calibration data, as it is based on a theoretical model which describes the signal distribution of the optical photons collected by the photodetector array. This PET concept aims to achieve equivalent performance to existing systems at a lower cost.

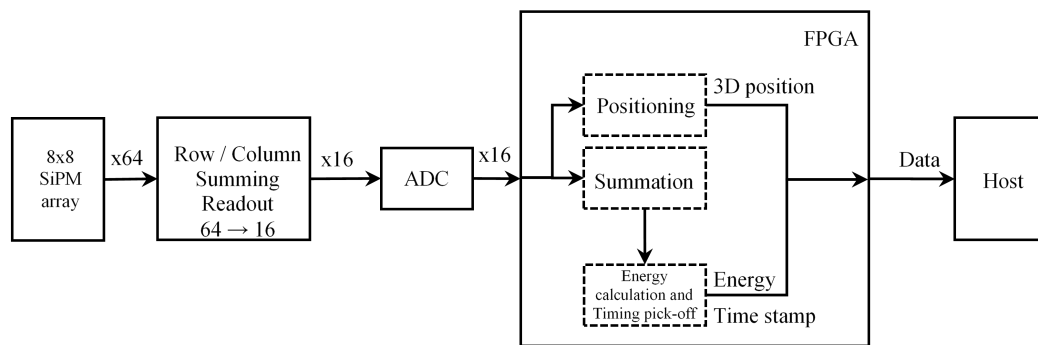


Figure 7. Block diagram of the FPGA-based data acquisition module.

Acknowledgments

This work was supported by Brazilian Nuclear Energy Commission (CNEN) and São Paulo Research Foundation (FAPESP grant #16/21345-4). The authors thank Yuri Musienko for providing the SiPM pre-amplifier circuit schematics.

References

- [1] M. Pizzichemi, *Positron Emission Tomography: state of the art and future developments*, 2016 *JINST* **11** C08004.
- [2] D.A.B. Bonifacio, N. Belcari, S. Moehrs, M. Moralles, V. Rosso, S. Vecchio et al., *A time efficient optical model for GATE simulation of a LYSO scintillation matrix used in PET applications*, *IEEE Trans. Nucl. Sci.* **57** (2010) 2483.
- [3] D.R. Schaart, S. Seifert, R. Vinke, H.T. van Dam, P. Dendooven, H. Löhner et al., *LaBr3:ce and SiPMs for time-of-flight PET: achieving 100 ps coincidence resolving time*, *Phys. Med. Biol.* **55** (2010) N179.
- [4] G. Ariño-Estrada, G. S. Mitchell, S. I. Kwon, J. Du, H. Kim, L.J. Cirignano et al., *Towards time-of-flight PET with a semiconductor detector*, *Phys. Med. Biol.* **63** (2018) 04LT01.
- [5] S. España, R. Marcinkowski, V. Keereman, S. Vandenberghe and R.V. Holen, *DigiPET: sub-millimeter spatial resolution small-animal PET imaging using thin monolithic scintillators*, *Phys. Med. Biol.* **59** (2014) 3405.
- [6] D.A.B. Bonifacio, E. Gros-Daillon and L. Verger, *Microscale mapping of SPAD photon detection probability*, 2017 *JINST* **12** P05010.
- [7] S.E. Brunner et al., *A comprehensive characterization of the time resolution of the Philips Digital Photon Counter*, 2016 *JINST* **11** P11004.
- [8] C. Xu, *Study of the silicon photomultipliers and their applications in Positron Emission Tomography*, Ph.D. Thesis, Universität Hamburg (2014) [https://inis.iaea.org/search/search.aspx?orig_q=RN:45076521].
- [9] L. Njejmama, M.-A. Tetrault, L. Arpin, A. Burghgraeve, P. Maille, J.-C. Lavoie et al., *Design of a real-time FPGA-based DAQ architecture for the LabPET II, an APD-based scanner dedicated to small animal PET imaging*, in proceedings of the *18th IEEE-NPSS Real Time Conference*, Berkeley, CA, U.S.A., 2012, pp. 1–5.
- [10] M.D. Rolo et al., *TOFPET ASIC for PET applications*, 2013 *JINST* **8** C02050.
- [11] A. Aguilar et al., *Pilot tests of a PET detector using the TOF-PET ASIC based on monolithic crystals and SiPMs*, 2016 *JINST* **11** C12033.
- [12] A. Tontini et al., *Design and characterization of a low-cost FPGA-based TDC*, *IEEE Trans. Nucl. Sci.* **65** (2018) 680.
- [13] J.W. Young et al., *FPGA based front-end electronics for a high resolution PET scanner*, *IEEE Nucl. Sci. Symp. Conf. Rec.* **M3-22** (1999) 902.
- [14] A. Bousselham, *FPGA based data acquisition and digital pulse processing for PET and SPECT*, Ph.D. Thesis, Stockholm University (2007) [<http://urn.kb.se/resolve?urn=urn:nbn:se:su:diva-6618>].
- [15] J. Imrek, D. Novak, G. Hegyesi, G. Kalinka, J. Molnar, J. Vegh et al., *Development of an FPGA-based data acquisition module for small animal PET*, *IEEE Trans. Nucl. Sci.* **53** (2006) 2698.
- [16] M. Haselman et al., *FPGA-based pulse parameter discovery for positron emission tomography*, *IEEE Nucl. Sci. Symp. Conf. Rec.* **M06-1** (2009) 2956.
- [17] R. Pedro et al., *The MiniPET: a didactic PET system*, 2012 *JINST* **8** C03005.

- [18] R. Fontaine, F. Lemieux, N. Viscogliosi, M.-A. Tetrault, M. Bergeron, J. Riendeau et al., *Timing improvement by low-pass filtering and linear interpolation for the LabPETTM scanner*, in proceedings of the *15th IEEE-NPSS Real-Time Conference*, Batavia, IL, U.S.A., 2007, pp. 1-5.
- [19] W. Hu et al., *A simple and improved digital timing method for positron emission tomography*, *Nucl. Instrum. Meth. A* **622** (2010) 219.
- [20] L.S. Jorge, D. Bonifacio, D. DeWitt and R. Miyaoka, *Experimental validation of improved 3D SBP positioning algorithm in PET applications using UW Phase II Board*, *Nucl. Instrum. Meth. A* **838** (2016) 103.
- [21] J. Yang et al., *Update on time-of-flight PET imaging*, *2018 JINST* **13** P04008.
- [22] K. Shibuya, F. Nishikido, T. Tsuda, T. Kobayashi, C. Lam, T. Yamaya et al., *Timing resolution improvement using DOI information in a four-layer scintillation detector for TOF-PET*, *Nucl. Instrum. Meth. A* **593** (2008) 572.
- [23] M.A. Nelson, B.D. Rooney, D.R. Dinwiddie and G.S. Brunson, *Analysis of digital timing methods with BaF₂ scintillators*, *Nucl. Instrum. Meth. A* **505** (2003) 324.
- [24] M. Streun, G. Brandenburg, H. Larue, E. Zimmermann, K. Ziemons and H. Halling, *Coincidence detection by digital processing of free-running sampled pulses*, *Nucl. Instrum. Meth. A* **487** (2002) 530.
- [25] CAEN SpA, *Digital Pulse Processing in Nuclear Physics rev. 3*, White Paper WP2018, Viareggio, 2011.
- [26] W.R. Leo, *Techniques for nuclear and particle physics experiments. A how-to approach*, Springer-Verlag, Berlin (1987).
- [27] G.F. Knoll, *Radiation detection and measurements*, John Wiley & Sons, Inc., New Jersey (2010).
- [28] T.J. Paulus, *Fast timing methods with scintillation detectors*, *IEEE Trans. Nucl. Sci.* **32** (1985) 1242.
- [29] M. Nakhostin, *Signal processing for radiation detectors*, John Wiley & Sons, Inc., New Jersey (2018).
- [30] W. Moses, *Trends in PET imaging*, *Nucl. Instrum. Meth. A* **471** (2001) 209.
- [31] G. Sportelli, N. Belcari, P. Guerra, F. Spinella, G. Franchi, F. Attanasi et al., *Reprogrammable acquisition architecture for dedicated positron emission tomography*, *IEEE Trans. Nucl. Sci.* **58** (2011) 695.
- [32] D. R. Schaart, H. T. van Dam, S. Seifert, R. Vinke, P. Dendooven, H. Löhner et al., *A novel, SiPM-array-based, monolithic scintillator detector for PET*, *Phys. Med. Biol.* **54** (2009) 3501.
- [33] R. Verheyden, H. Chagani, R. Dolenc, R. Pestotnik, P. Križan, S. Korpar et al., *Performance study of silicon photomultipliers as photon detectors for PET*, *Nucl. Instrum. Meth. A* **628** (2011) 381.
- [34] V.C. Spanoudaki, A.B. Mann, I. Konorov, I. Torres-Espallardo, S. Paul, S.I. Ziegler et al., *Use of single photon counting detector arrays in combined PET/MR: Characterization of LYSO-SiPM detector modules and comparison with a LSO-APD detector*, *2007 JINST* **2** P12002.
- [35] J. Du, J. P. Schmall, K. Di, Y. Yang, M. Judenhofer, J. Bec et al., *Design and optimization of a high-resolution PET detector module for small-animal PET based on a 12 × 12 silicon photomultiplier array*, *Biomed. Phys. Eng. Express* **1** (2015) 045003.
- [36] H.-J. Choe, Y. Choi, W. Hu, J. Yan and J.H. Jung, *Development of capacitive multiplexing circuit for SiPM-based time-of-flight (TOF) PET detector*, *Phys. Med. Biol.* **62** (2017) N120.

- [37] J. Du, X. Bai, A. Gola, F. Acerbi, A. Ferri, C. Piemonte et al., *Performance of a high-resolution depth-encoding PET detector module using linearly-graded SiPM arrays*, *Phys. Med. Biol.* **63** (2018) 035035.
- [38] G.B. Saha, *Basic of PET imaging — Physics, chemistry and regulations*, Springer Science+Business Media, LLC, New York (2010).
- [39] M. Streun, G. Brandenburg, M. Khodaverdi, H. Larue, C. Parl and K. Ziemons, *Timemark correction for the ClearPETTM scanners*, *IEEE Nucl. Sci. Symp. Conf. Rec.* **M07-155** (2005) 2057.
- [40] K. Ziemons, E. Auffray, R. Barbier, G. Brandenburg, P. Bruyndonckx, Y. Choi et al., *The ClearPETTM project: development of a 2nd generation high-performance small animal PET scanner*, *Nucl. Instrum. Meth. A* **537** (2005) 307.
- [41] T.K. Lewellen, D. DeWitt, R.S. Miyaoka and S. Hauck, *A building block for nuclear medicine imaging systems data acquisition*, *IEEE Trans. Nucl. Sci.* **61** (2014) 79.
- [42] W. Hu, Y. Choi, K. J. Hong, J. Kang, J. H. Jung, Y. S. Huh et al., *Free-running ADC- and FPGA-based signal processing method for brain PET using GAPD arrays*, *Nucl. Instrum. Meth. A* **664** (2012) 370.
- [43] D.A.B. Bonifacio and M. Morales, *Modeling of 3D gamma interaction position in a monolithic scintillator block with a row-column summing readout*, *IEEE Nucl. Sci. Symp. Conf. Rec.* **M10-22** (2012) 2606.